DOI:10.1158/0008-5472.CAN-05-3781

Cancer Research

A Critical Role for the Inflammatory Response in a Mouse Model of Preneoplastic Progression

Kathryn L. Schwertfeger, Wa Xian, Alan M. Kaplan, et al.

Cancer Res 2006;66:5676-5685. Published online June 1, 2006.

DOI:10.1158/0008-5472.CAN-05-3781

Research Article

A Critical Role for the Inflammatory Response in a Mouse Model of Preneoplastic Progression

Kathryn L. Schwertfeger,[1] Wa Xian,[1] Alan M. Kaplan,[2] Sandra H. Burnett,[3] Donald A. Cohen,[2] and Jeffrey M. Rosen[1]

[1]Department of Molecular and Cellular Biology, Baylor College of Medicine, Houston, Texas; [2]Department of Microbiology, Immunology, and Molecular Genetics, University of Kentucky, Lexington, Kentucky; and [3]Department of Microbiology and Molecular Biology, Brigham Young University, Provo, Utah

Abstract

The tumor microenvironment, which includes inflammatory cells, vasculature, extracellular matrix, and fibroblasts, is a critical mediator of neoplastic progression and metastasis. Using an inducible transgenic mouse model of preneoplastic progression in the mammary gland, we discovered that activation of inducible fibroblast growth factor receptor-1 (iFGFR1) in the mammary epithelium rapidly increased the expression of several genes involved in the inflammatory response. Further analysis revealed that iFGFR1 activation induced recruitment of macrophages to the epithelium and continued association with the alveolar hyperplasias that developed following long-term activation. Studies using HC-11 mammary epithelial cells showed that iFGFR1-induced expression of the macrophage chemoattractant osteopontin was required for macrophage recruitment *in vitro*. Finally, conditional depletion of macrophages inhibited iFGFR1-mediated epithelial cell proliferation and lateral budding. These findings show that inflammatory cells, specifically macrophages, are critical for mediating early events in an inducible transgenic mouse model of preneoplastic progression. (Cancer Res 2006; 66(11): 5676-85)

Introduction

Tumor progression and metastasis are strongly influenced by the microenvironment, which includes inflammatory cells, vasculature, extracellular matrix (ECM), and fibroblasts (1, 2). The relationship between inflammation and cancer has been well correlated in studies focusing on the role of chronic inflammation on cancer predisposition. There are several chronic inflammatory conditions, such as inflammatory bowel disease, *Helicobacter pylori* infection, hepatitis B or C infection, and prostatitis, which result in predisposition to specific cancers, such as colon cancers, gastric cancers, liver carcinomas, and prostate carcinomas, respectively (3). Studies of these and other systems have shown that following recruitment to tumors, inflammatory cells, including macrophages, are able to enhance tumor growth and progression by expressing growth factors, ECM remodeling enzymes, and angiogenic factors (3, 4).

Fibroblast growth factors (FGF) and their receptors (FGFR) have been implicated in a wide range of cellular and biological functions, including proliferation, survival, differentiation, migration, and angiogenesis (5, 6) Inappropriate FGF signaling has been linked to tumor development in models of mammary, prostate, skin, and urothelial cancers (7). In the murine mammary gland, several FGFs (FGF-3, FGF-4, and FGF-8) have been identified as oncogenes based on studies of proviral insertion of the mouse mammary tumor virus (MMTV; refs. 8–11). In human breast cancer, studies have shown elevated FGF-8 mRNA in a few malignant breast tumors (12). In addition, amplification or activation of FGFR1, FGFR2, and FGFR4 has been identified in human breast cancer (13). Taken together, these data suggest that deregulation of the FGF signaling axis may contribute to breast tumorigenesis.

To examine the role of FGF signaling in mammary tumorigenesis, we previously developed transgenic mice that express an inducible FGFR1 (iFGFR1), which is activated following chemically induced dimerization, in mammary epithelial cells (14). Activation of iFGFR1 in the mammary gland resulted in the initial development of lateral buds along the mammary ducts within 3 days of treatment followed by the development of hyperplasias within 4 weeks of treatment, which progressed to multicellular, invasive lesions following 4 to 6 weeks of sustained activation. These later stage lesions exhibited ECM remodeling and increased angiogenesis surrounding the lesions, suggesting that iFGFR1 activation could induce changes in the microenvironment. Due to the ability to temporally control the formation of hyperplastic lesions in MMTV-iFGFR1 transgenic mice, these mice represent a unique model in which we can examine the role of the microenvironment in the early stages of tumorigenesis. In the studies described here, we characterize the early events of iFGFR1-induced preneoplastic progression by identifying genes that were induced in the mammary gland following short-term activation of iFGFR1. A number of these induced genes are involved in the immune response, and our studies show that macrophages are associated with and required for both epithelial proliferation and angiogenesis in this model.

Materials and Methods

Animals. The generation of iFGFR1 transgenic mice has been described previously (14). MaFIA transgenic mice, the generation of which has been described previously (15), were obtained from The Jackson Laboratory (Bar Harbor, ME). Animal care and procedures were approved by the Institutional Animal Care and Use Committee of Baylor College of Medicine (Houston, TX) and were in accordance with the procedures detailed in the Guide for Care and Use of Laboratory Animals (NIH publication 85-23).

Dimerizer treatment, mammary gland isolation, histology, and epithelial budding quantitation. Six-week-old mice were injected i.p. with 1 mg/kg AP20187 (Ariad Pharmaceuticals, Cambridge, MA) every 3 days. Mice were sacrificed at 8, 12, 16, 24, and 48 hours and 4 weeks after injection, and mammary glands from at least three mice were analyzed per

Note: Supplementary data for this article are available at Cancer Research Online (http://cancerres.aacrjournals.org/).

Requests for reprints: Jeffrey M. Rosen, Baylor College of Medicine, One Baylor Plaza, Houston, TX 77030. Phone: 713-798-6210; Fax: 713-798-8012; E-mail: jrosen@bcm.tmc.edu.

doi:10.1158/0008-5472.CAN-05-3781

DOI:10.1158/0008-5472.CAN-05-3781

time point. For the macrophage ablation studies, mice were injected with 10 mg/kg AP20187 daily for 5 days and every other day for a total treatment time of 9 days. At least five single and bigenic mice were analyzed. Mammary glands were fixed for 2 hours in 4% paraformaldehyde and either stained with hematoxylin as described previously (16) or embedded in paraffin and H&E stained using standard histologic protocols. To quantify epithelial budding structures, six images were taken per mammary gland section at ×10 magnification. Two sections were analyzed per gland, each ~100 μm apart to compensate for variability within the gland. The total number of epithelial structures was counted and expressed as a percentage of structures that contain epithelial buds. At least three mice and 200 epithelial structures were analyzed for each genotype.

Mammary epithelial cell preparation. Mammary glands were collected and pooled from three mice per time point treated for 0, 8, 16, and 24 hours with AP20187 and used to enrich for mammary epithelial cells as described previously (17). The resulting pellets were lysed with Trizol (Invitrogen, Carlsbad, CA), and RNA was extracted following the manufacturer's protocols.

RNA isolation and microarray analysis. For microarray analysis, histologic analysis of one of the inguinal (no. 4) mammary glands from each mouse was done, and glands from mice that showed any abnormalities, such as precocious lateral budding, in the absence of dimerizer treatment were not used in the analysis. RNA was isolated from the remaining fourth inguinal mammary gland from a total of seven mice per time point, and either pooled or individual samples were analyzed on four separate microarray chips. Mammary glands from 6-week-old mice that were treated for 8, 16, and 24 hours as well as from nontreated transgenic mice were isolated, the lymph nodes were removed, and the mammary glands were ground under liquid nitrogen and lysed in 2 mL Trizol. Following homogenization using a Polytron homogenizer, RNA was extracted using the standard protocol followed by additional column purification (RNeasy, Qiagen, Valencia, CA). Total RNA (5 μg) was labeled according to the manufacturer's recommendations (Affymetrix, Santa Clara, CA) and hybridized to MGU74Av2 chips (Affymetrix) in the Baylor Microarray Core Facility. Microarray Suite 5.0 was used initially to evaluate quality control by comparing 3′/5′ ratios of glyceraldehyde-3-phosphate dehydrogenase, which ranged from 1 to 2.63, and scaling factors, which ranged from 3.72 to 6.85, among chips. All analyses were done using GeneSpring (Silicon Genetics, Palo Alto, CA). Genes that were called absent or had expression values <20 in all time points were discarded. Genes that were either up-regulated or down-regulated were identified by doing a crosswise comparison of each treated sample compared with each 0 hour time point (16 comparisons) as well as comparing averages from pooled values at each time point, and genes with Ps < 0.05 were chosen for further analysis. Clustering analyses were done using k-means clustering algorithm in GeneSpring, and gene ontology analysis was done using the database for annotation, visualization, and integrated discovery (DAVID)/expression analysis systematic explorer (EASE) annotation tool.[4] All microarray experiments were done in accordance with minimum information about a microarray experiment standards, and the data have been deposited in the National Center for Biotechnology Information Gene Expression Omnibus data repository.[5]

Immunohistochemistry and immunofluorescence. The following antibodies and dilutions were used for immunohistochemistry: mouse monoclonal anti-hemagluttinin (HA) epitope (1:300; Covance Research Products, Denver, PA), rat monoclonal anti-F4/80 (1:200; Caltag Laboratories, Burlingame, CA), mouse monoclonal green fluorescent protein (GFP) Alexa Fluor 488 (1:500; Molecular Probes, Carlsbad, CA), goat polyclonal Ki67 (sc-7846, 1:500; Santa Cruz Biotechnology, Santa Cruz, CA), and rabbit polyclonal von Willebrand factor (VWF; 1:400; DakoCytomation, Carpinteria, CA). Immunostaining was done either without antigen retrieval (F4/80) or with sodium citrate antigen retrieval as described previously (HA, GFP, and Ki67; ref. 17). Antigen retrieval with the VWF antibody was done by boiling the slides for 20 minutes in 10 mmol/L Tris/1 mmol/L EDTA. GFP and Ki67-positive cells were counted and calculated relative to the number of total epithelial cells. At least 2,000 cells were counted for each data set. To count VWF-positive blood vessels, six fields were taken at ×20 magnification and both the large (>20 μm) and the small (<20 μm) blood vessels, specifically associated with epithelial structures, were counted. At least three mice per genotype (six iFGFR1/MaFIA mice were analyzed to obtain enough budding structures) and ~100 blood vessels per genotype were counted.

Fluorescence-activated cell sorting analysis. To analyze mammary glands for F4/80-positive cells, the fourth inguinal mammary glands were removed from wild-type (WT), MaFIA, and bigenic mice following the 10-day treatment protocol described above. The glands were minced and incubated with 2 mg/mL collagenase A (Roche, Indianapolis, IN) and 300 μg/mL hyaluronidase (Sigma-Aldrich, St. Louis, MO) for 3 hours at 120 rpm. Following digestion, the cells were washed thrice at 1,500 rpm. The cells were then resuspended in HBSS plus 0.5% fetal bovine serum (HBSS+) at a concentration of 1×10^6/mL and incubated with phycoerythrin-conjugated F4/80 (1:200; Caltag Laboratories) for 20 minutes on ice. The cells were washed with HBSS+ at 1,500 rpm and filtered through a 40-μm filter (Falcon, Morristown, TN) before fluorescence-activated cell sorting (FACS) analysis using a Beckman-Coulter (Fullerton, CA) Epics XL in the Baylor Flow Cytometry Core.

Quantitative reverse transcription-PCR. RNA was extracted from HC-11 cells using Trizol as recommended by the manufacturer. Samples of RNA (5 μg) were treated with DNase I as recommended by the manufacturer (Invitrogen) followed by generation of cDNA using SuperScript II (Invitrogen). One tenth of the final reaction volume was used in quantitative PCRs as described previously (18) using the ABI (Foster City, CA) Prism 7500 thermocycler. Relative quantitation of the expression of each gene was calculated and normalized to cyclophilin expression levels using the $2^{-\Delta\Delta Ct}$ method (19). The following primer sequences were used: 5′-CTTTCACTCCAATCGTCC-3′ and 5′-CCTTTCCGTTGTTGTTCCTG-3′ (osteopontin) and 5′-TGAGCACTGGGGAGAAAGG-3′ and 5′TTGCCA-TCCAGCCACTCAG-3′ (cyclophilin).

Cell culture and immunoblot analysis. HC-11 cells were maintained as described (14). Retroviral transduction of HC-11 cells with the pMMP-iFGFR1 and pMMP-Fv constructs has been described previously (14). The cells were incubated in serum-free RPMI 1640 for 16 hours before treatment with 30 nmol/L AP20187. Medium was collected at the indicated times and filtered using a 0.45-μm filter. The medium was concentrated using YM50 Microcon protein concentrators (Millipore, Billerica, MA), and protein assays were done using the Bio-Rad (Hercules, CA) protein assay reagent. Total protein (10 μg amounts) was immunoblotted with anti-osteopontin (sc-10593, 1:1,000; Santa Cruz Biotechnology) as described previously (16). Equal loading was assessed by staining the membrane with Ponceau S before immunoblot analysis.

Migration assay in HC-11 cells. Conditioned medium was collected from HC-11/iFGFR1 cells after 24 hours of dimerizer treatment and filtered as described above. Medium (0.5 mL) was added to wells of a 12-well plate (Falcon). RAW 264.7 cells (40,000; American Type Culture Collection, Rockville, MD) were plated in 0.5 mL serum-free DMEM (Invitrogen) in 12-well format cell culture inserts containing 8 μm pores (Falcon). Following a 24-hour incubation, cells that had not migrated through the filters were removed using a cotton swab and the filters were stained with hematoxylin. The cells were counted, and the amount of cells that had migrated in response to medium from dimerizer treated cells was normalized to the number of cells that had migrated in response to nontreated cells. Quantitation was done on four independent experiments. To inhibit osteopontin activity, an osteopontin-blocking antibody, MPIIIB10$_1$ (Developmental Studies Hybridoma Bank, University of Iowa, Iowa City, IA), was added to the medium at a concentration of 7.2 μg/mL and rocked for 20 minutes to distribute the antibody before adding to the 12-well plates.

Results

Activation of iFGFR1 induces lateral budding after 24 to 48 hours of dimerizer treatment. To characterize the timing of the onset of lateral bud formation induced by iFGFR1 activation,

[4] http://apps1.niaid.nih.gov/david/.
[5] http://www.ncbi.nlm.nih.gov/geo/.

DOI:10.1158/0008-5472.CAN-05-3781

6-week-old iFGFR1 transgenic mice were treated with dimerizer for 8, 24, and 48 hours and both terminal end bud (TEB) and ductal morphology were analyzed by H&E staining. Mammary glands from nontreated transgenic mice exhibited normal TEBs and ducts with no evidence of lateral budding (Fig. 1*A, a* and *d*). Following 8 hours of dimerizer treatment, the structure of the TEBs still seemed comparable with TEBs observed in nontreated iFGFR1 transgenic mice (Fig. 1*A, b*). No distinct budding was observable around the ducts; however, the stroma appeared thicker than stroma typically observed in mammary glands from nontransgenic mice (Fig. 1*A, d* and *e, arrows*). Following 24 hours of dimerizer treatment, epithelial buds started to appear along the neck of the TEB and the ducts (data not shown) and were well established by 48 hours of treatment (Fig. 1*A, c* and *f, arrowheads*). Finally, treatment of nontransgenic littermates with dimerizer for equivalent amounts of time did not result in any changes in epithelial structure (data not shown).

The iFGFR1 construct was generated with a HA epitope tag on the COOH terminal of the protein to facilitate identification of transgene-positive cells (14). To examine the localization of transgene-positive cells, sections were stained with a HA antibody. Although there was no observable staining in the epithelial cells from nontransgenic mice (Fig. 1*B, a*), mammary glands from nontreated iFGFR1 transgenic mice exhibited punctate epithelial staining of HA-positive cells (Fig. 1*B, b, arrow*). After 8 hours of treatment, HA-positive cells were found in clusters containing two to three cells in the ductal epithelium (Fig. 1*B, c, arrow*), and by 48 hours the lateral buds that had formed along the duct appeared to consist primarily of HA-positive cells (Fig. 1*B, d*).

As described previously (14), mammary tumors were observed in transgenic mice following multiple pregnancies. These mammary tumors were characterized as squamous adenocarcinomas, and immunostaining with the HA antibody revealed that the tumor cells are transgene positive (Supplementary Fig. S1). Although these mice were not treated with dimerizer, we have observed that high levels of transgene expression, such as the levels induced by the hormone-responsive MMTV promoter during pregnancy, can result in drug-independent activation of iFGFR1 (data not shown). Therefore, activation of iFGFR1 in the mammary epithelium increases the susceptibility of these mice to form mammary tumors.

Identification of genes regulated by iFGFR1 following short-term treatment. To identify genes that may be mediating the early events of lateral bud formation, microarray analysis was done on RNA extracted from mammary glands of 6-week-old iFGFR1 transgenic mice following 0, 8, 16, and 24 hours of dimerizer treatment. We identified a total of 342 genes that were either up-regulated or down-regulated by iFGFR1 at any time point compared with nontreated transgenic mice (Supplementary Table S1). To analyze the temporal regulation of the genes being induced by iFGFR1, the k-means clustering algorithm in GeneSpring was used to cluster genes based on their expression patterns over time (Fig. 2). This analysis identified five clusters of genes with differing expression profiles (Fig. 2; Supplementary Table S2). Strikingly, the majority of the genes (88%) were significantly increased by 8 hours, which was the earliest time point examined.

Gene ontology analysis of the genes in each cluster revealed that the majority of the classified genes that were induced in cluster 1 were transcription factors. In addition, genes that are involved in angiogenesis, cytoplasm organization and biogenesis, cell cycle, and small GTPase signal transduction were identified in this cluster. Although some transcription factors were also found in cluster 2, the majority of the genes that were induced in this cluster were associated with the inflammatory response, including the macrophage chemoattractant RANTES/Ccl5. This cluster also included genes involved in signal transduction, apoptosis, chemotaxis, and cell cycle regulation. Cluster 3 contained a smaller number of genes primarily involved in metabolic activity. Of interest, two known macrophage chemoattractants were identified

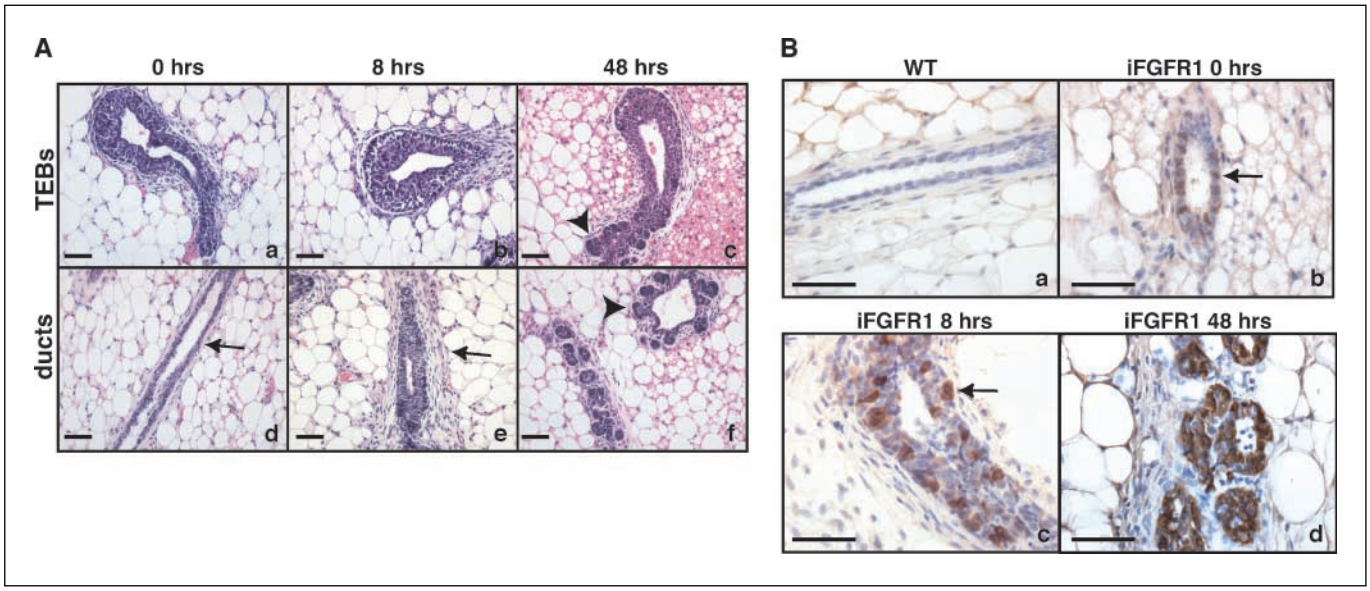

Figure 1. Rapid induction of lateral budding following iFGFR1 activation in mammary epithelial cells. *A,* H&E-stained mammary glands sections showing TEBs (*a-c*) and ducts (*d-f*) from nontreated and treated iFGFR1 transgenic mice. Mammary gland sections from nontreated iFGFR1 mice (*a* and *d*) and from mice following 8 (*b* and *e*) and 48 hours (*c* and *f*) of dimerizer treatment. *d* and *e, arrows,* stroma surrounding the ducts. *c* and *f, arrowheads,* lateral budding from the epithelium. *B,* immunohistochemical analysis of mammary gland sections from WT (*a*) and iFGFR1 mice (*b-d*) treated with dimerizer for 0, 8, and 48 hours using an anti-HA antibody. *Arrows,* single HA-positive cells (*b*) and small clusters of HA-positive cells (*c*) within the epithelium. Bar, 50 μm.

DOI:10.1158/0008-5472.CAN-05-3781

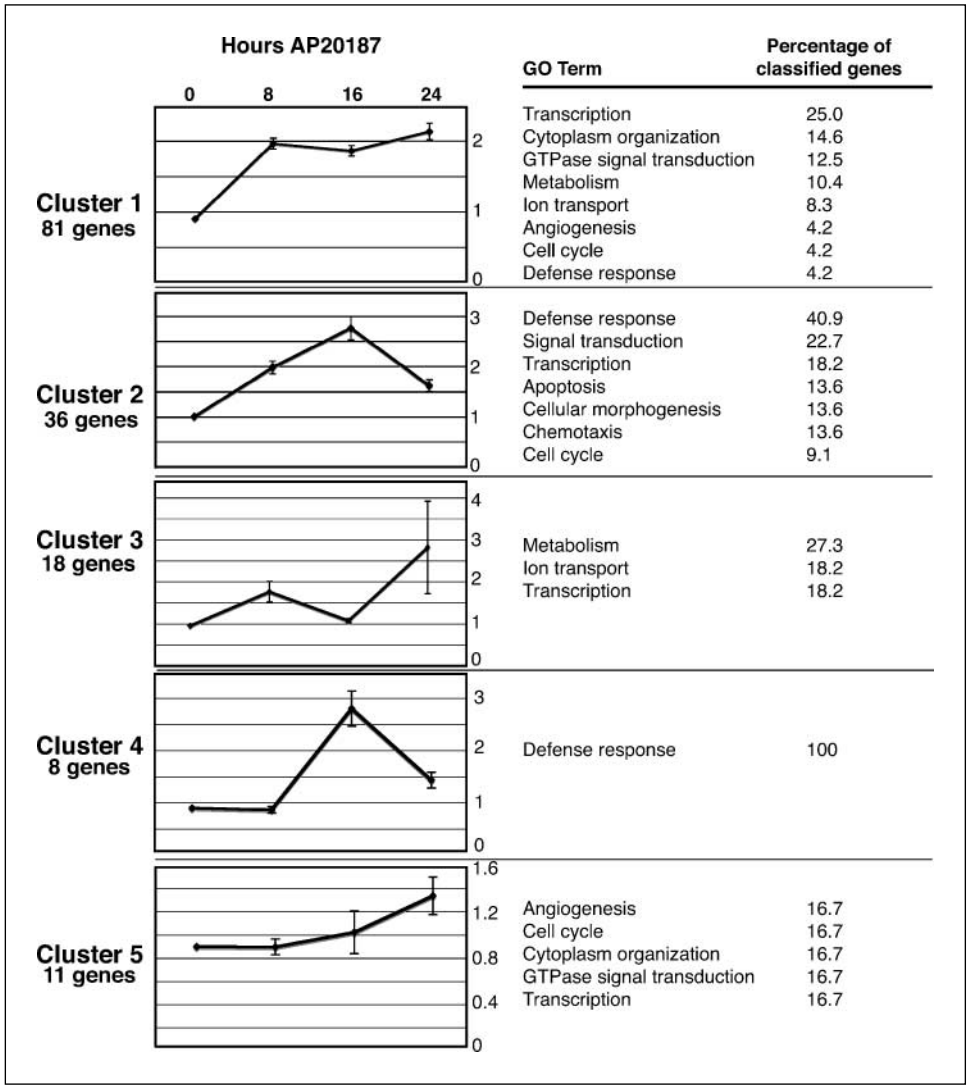

Figure 2. Cluster analysis of genes identified by microarray analysis, which are induced following dimerizer treatment. Samples were clustered by k-means clustering. *Right,* values in each cluster were averaged and plotted. *Y axis,* fold change of expression. *Bars,* SE. The number of genes represented in each cluster is indicated below the cluster name. Gene ontology (*GO*) analysis was done on each gene cluster using DAVID/EASE,[4] and gene ontology groups containing at least two genes are listed for each cluster. The percentage of classified genes is listed for each gene ontology group.

in this cluster, osteopontin and macrophage chemoattractant protein-1/Ccl2. The only genes in cluster 4 that were classified using gene ontology terms are involved in defense response. Finally, several of the genes identified in cluster 5 belong to gene ontology groups that were identified in the previous clusters, including angiogenesis, cell cycle regulation, cytoplasm organization and biogenesis, GTPase signal transduction, and transcription. Together, these data suggest that iFGFR1 activation in the epithelium induces the expression of genes involved in several processes associated with tumor formation, including blood vessel formation, cell cycle regulation, migration, signal transduction, chemotaxis, and the inflammatory response.

Increased macrophage accumulation around the epithelium following 8 hours of iFGFR1 activation. Because the induction of at least three known macrophage chemoattractants, RANTES, Ccl2, and osteopontin, was observed, the effects of iFGFR1 activation on macrophage recruitment were examined by immunostaining with the F4/80 antibody. Although the F4/80 antibody stains both macrophages and eosinophils, these two cell types can be distinguished based on nuclear morphology. Examination of epithelial structures in the mammary gland revealed a dramatic increase in the number of macrophages surrounding the ducts from iFGFR1 mice following 8 and 24 hours of dimerizer treatment (Fig. 3*B* and *D*) compared with those from similarly treated nontransgenic littermates (Fig. 3*A* and *C, arrow*). Macrophages continued to associate with the epithelium following 4 weeks of dimerizer treatment. As shown in Fig. 3*F*, the macrophages were intercalated into the epithelium and appeared to be in close proximity to the epithelial buds, similar to macrophage localization observed during pregnancy (Fig. 3*E*; ref. 20).

Based on the observation that iFGFR1 activation induced macrophage recruitment, the recruitment of other immune response cells was examined. Antibodies to B cells, T cells, and neutrophils revealed no significant recruitment of these cells types to the epithelium following either short-term (8, 24, and 48 hours) or long-term (4 week) iFGFR1 activation (data not shown).

iFGFR1 activation results in increased gene expression of osteopontin in the mammary gland and in HC-11 cells. Due to the increase in macrophage accumulation surrounding the epithelium following dimerizer treatment, we examined the expression levels of the macrophage chemoattractants identified by gene array analysis. Quantitative reverse transcription-PCR (RT-PCR) analysis confirmed that the expression of osteopontin, Ccl2, and RANTES was increased by 8 hours in the mammary

DOI:10.1158/0008-5472.CAN-05-3781

gland (Fig. 4*A*; data not shown). However, only osteopontin was induced in an enriched preparation of mammary epithelial cells that was isolated from mammary gland tissue following dimerizer treatment of transgenic mice (Fig. 4*A*; data not shown), suggesting that Ccl2 and RANTES are being induced by a paracrine mechanism.

Although the mammary epithelial cell preparation enriches for epithelial cells, it is possible that osteopontin may be expressed in the small percentage of contaminating cells. Therefore, we further analyzed the induction of osteopontin in the mouse mammary epithelial cell line HC-11 (21), which was transduced with a retrovirus encoding iFGFR1 as described previously (14). To determine whether iFGFR1 induces osteopontin expression and secretion, mock-transduced cells and cells expressing either the Fv domain alone or iFGFR1 were treated with dimerizer for 6 and 24 hours. Quantitative PCR of RNA isolated from these cells showed an increase in osteopontin expression following iFGFR1 activation (data not shown). In addition, conditioned medium was collected and analyzed for osteopontin expression using immunoblot analysis. As shown in Fig. 4*B*, secreted osteopontin was detected by 6 hours and further increased by 24 hours of dimerizer treatment in cells expressing iFGFR1 but not in mock-transduced cells or cells expressing the Fv domain alone.

iFGFR1-induced secretion of osteopontin is necessary for macrophage migration. To assess the ability of iFGFR1-induced osteopontin to induce macrophage migration, we did a migration assay using HC-11/iFGFR1-conditioned medium and the RAW 264.7 macrophage cell line. After 24 hours of dimerizer treatment, medium was collected from mock-transduced cells, HC-11/Fv, and HC-11/iFGFR1 cells, and the ability of RAW 264.7 cells to migrate in response to the conditioned medium was quantified (Fig. 4*C*). Compared with conditioned medium from dimerizer-treated mock-transduced and HC-11/Fv cells, conditioned medium from dimerizer-treated HC-ll/iFGFR1 cells significantly increased the number of macrophages that were able to migrate ($P < 0.05$).

To determine whether iFGFR1-induced macrophage migration is dependent on the presence of functional osteopontin, an antibody that has been shown to block osteopontin activity, MPIIIB10$_1$ (22), was added to the conditioned medium before doing the migration assay. As shown in Fig. 4*C*, addition of the osteopontin-blocking antibody, but not a mouse IgG1 isotype control, significantly reduced the number of macrophages that migrated in response to conditioned medium ($P < 0.05$). These data suggest that, in a mammary epithelial cell model, iFGFR1-induced macrophage migration can be mediated by secreted osteopontin.

Macrophages are required for the iFGFR1-induced lateral budding phenotype. To determine whether macrophages are required for the development of the iFGFR1-induced lateral budding phenotype, the MMTV-iFGFR1 transgenic mice were crossed

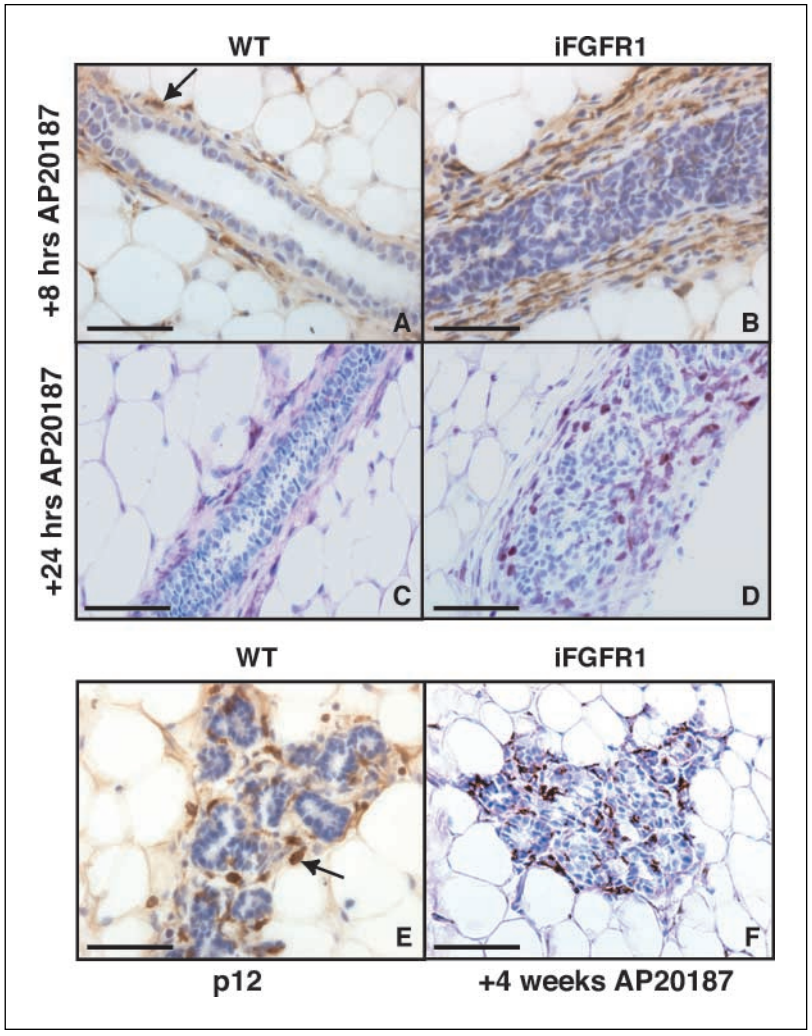

Figure 3. Increased macrophage accumulation around the epithelium following both short-term and long-term iFGFR1 activation. *A,* F4/80 staining of mammary glands from WT mice treated with dimerizer for 8 hours. *B,* increased F4/80 staining surrounding ducts from iFGFR1 transgenic mice following 8 hours of dimerizer treatment. *C,* F4/80 staining of mammary gland sections from WT mice treated with dimerizer for 24 hours. *D,* increased macrophage staining surrounding ducts and the developing lateral buds following 24 hours of dimerizer treatment. *E,* numerous macrophages are associated with alveolar buds in mammary glands from midpregnant WT mice as shown by F4/80 staining. *F,* F4/80 staining of alveolar hyperplasias from iFGFR1 mice following 4 weeks of dimerizer treatment. Bar, 50 μm.

DOI:10.1158/0008-5472.CAN-05-3781

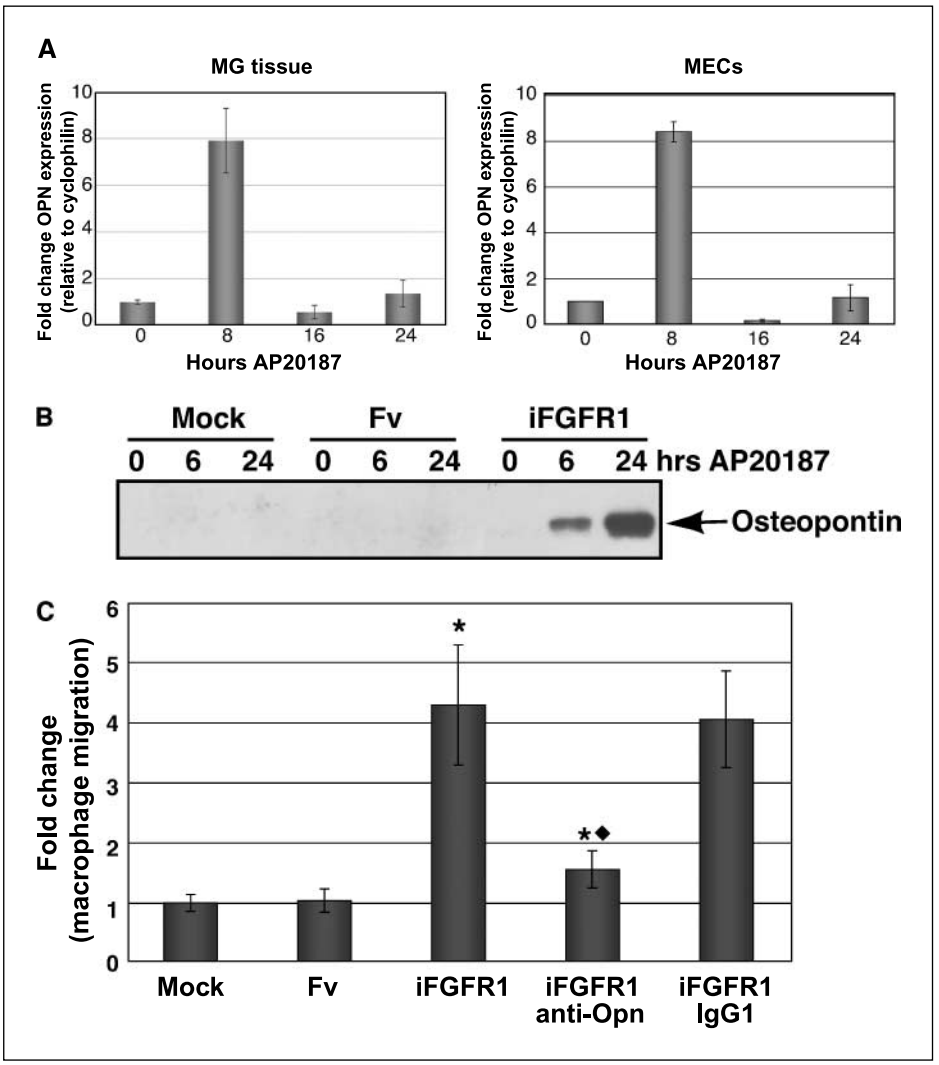

Figure 4. Osteopontin (*OPN*) is induced in mammary epithelial cells following iFGFR1 activation and is required for macrophage recruitment. *A,* quantitative PCR analysis of osteopontin expression in the mammary gland (*MG*; *left*) and mammary epithelial cells (*MECs*; *right*). Values were normalized to cyclophilin expression levels using the $\Delta\Delta C_t$ method and plotted as fold change with respect to RNA from nontreated mice (0 hour). *Bars,* SE. *B,* immunoblot analysis of osteopontin in conditioned medium from mock-transduced HC-11 cells, HC-11 cells expressing the Fv domain alone, and iFGFR1/HC-11 cells treated for 0, 6, and 24 hours with dimerizer. *C,* quantitation of hematoxylin-stained RAW 264.7 cells following migration assays using conditioned medium from mock-transduced HC-11 cells, HC-11 cells expressing the Fv domain alone, and HC-11/iFGFR1 cells treated with dimerizer for 24 hours. Conditioned medium was either not treated or incubated with anti-osteopontin antibody or an IgG1 isotype control before doing the migration assays. Each value is relative to the number of cells that migrated in response to conditioned medium from nontreated cells. *, $P < 0.05$, significant increase in the number of cells that migrated in response to medium from HC-11/iFGFR1 cells (paired *t* test). ♦, $P < 0.05$, significant decrease in the number of cells that migrated in response to the same medium containing anti-osteopontin antibody (paired *t* test). *Bars,* SE.

to MaFIA transgenic mice. MaFIA mice express a transgene in which enhanced GFP (EGFP) is driven by the c-fms promoter, which is targeted primarily to macrophages followed by an IRES-ΔLNGFR-FKBP-Fas suicide construct (15). The transgene contains the same dimerization domain as the iFGFR1 construct; therefore, dimerization and induction of Fas-based apoptosis in macrophages is mediated using the same synthetic dimerizer, AP20187. Studies of these mice have shown previously that dimerization of the transgene results in a significant reduction in the number of EGFP-expressing cells, including macrophages and dendritic cells, in several tissues.

To examine macrophage depletion in the mammary gland, mice were treated with dimerizer for 9 days and GFP-positive cells were counted following immunostaining with an anti-GFP antibody. Although mammary glands from nontransgenic mice exhibited very little staining (Fig. 5*A*), numerous GFP-positive cells were identified in mammary glands from nontreated MaFIA transgenic mice (Fig. 5*B*). However, treatment of both MaFIA transgenic and iFGFR1/MaFIA bigenic mice with dimerizer resulted in a significant decrease ($P < 0.05$) in the number of GFP-positive cells (Fig. 5*C* and *D*). To further analyze macrophage depletion, FACS analysis was done using the F4/80 antibody on cells isolated from the mammary glands of WT, iFGFR1, MaFIA, and iFGFR1/MaFIA bigenic mice following AP20187 treatment. As shown in Fig. 5*E*, there was a significant decrease ($P < 0.05$) in F4/80-positive cells in both MaFIA and iFGFR1/MaFIA bigenic mice following treatment. Consistent with observations in the initial studies describing these mice (15), there was a greater decrease in the amount of GFP-positive cells (60%) compared with the F4/80-positive cells (50%) possibly due to incomplete penetrance and/or variable expressivity of the transgene.

To examine TEB and ductal morphology, whole-mount analysis was done on mammary glands from AP20187-treated nontransgenic, MaFIA transgenic, and iFGFR1/MaFIA bigenic mice. TEBs from WT and MaFIA mice exhibited similar morphologies (Fig. 5*F* and *G*). As expected, TEBs from iFGFR1 transgenic mice exhibited extensive budding around the neck of the TEB (Fig. 5*H*). In comparison, TEBs from the iFGFR1/MaFIA bitransgenic mice exhibited less budding around the neck of the TEB than iFGFR1 alone (Fig. 5*I*). In addition, extensive lateral budding was observed along the subtending ducts in mammary glands from the iFGFR1 transgenic mice, consistent with previously published studies (Fig. 5*J*; ref. 14). Although lateral budding was also observed along the subtending ducts in mammary glands from iFGFR1/MaFIA transgenic mice, the extent of lateral budding along the ducts was diminished (Fig. 5*K*). To quantify this change in budding,

DOI:10.1158/0008-5472.CAN-05-3781

histologic sections were examined and the percentage of epithelial budding structures was determined (Fig. 6*A-D*). Although there was some budding observed in the iFGFR1/MaFIA bigenic animals (Fig. 6*C, arrow*), the budding observed in the iFGFR1 transgenic mice was more extensive (Fig. 6*B, arrow*). Quantification of the percentage of epithelial structures that exhibited the budding phenotype revealed a significant decrease ($P < 0.0001$) in the percentage of budding structures in the iFGFR1/MaFIA bigenic mice compared with the iFGFR1 transgenic mice (Fig. 6*D*). Interestingly, analysis of these histologic sections revealed a change in the adipose stroma in mammary glands from both MaFIA and iFGFR1/MaFIA bigenic mice (compare Fig. 6*A* and Fig. 6*B*), suggesting that the effects of the macrophages on the epithelium may be either direct or indirect through modulating changes in the stroma.

Macrophage depletion results in decreased iFGFR1-induced epithelial proliferation and angiogenesis. To further characterize the effects of macrophage depletion following iFGFR1 activation, the ability of iFGFR1 to induce proliferation was examined by immunostaining sections with an anti-Ki67 antibody. As shown in Fig. 6*E*, there was a significant decrease ($P < 0.01$) in the percentage of Ki67-positive epithelial cells in mammary glands from the iFGFR1/MaFIA bigenic mice compared with mice expressing the iFGFR1 transgene alone. These results are consistent with the decrease in epithelial budding and suggest that macrophages are important for iFGFR1-induced epithelial proliferation in the mammary gland.

As described previously (14), iFGFR1 activation in the mammary gland results in increased angiogenesis. To determine whether macrophages might be involved in mediating iFGFR1-induced angiogenesis, blood vessels were examined in mammary gland sections from dimerizer-treated WT, iFGFR1, and iFGFR1/MaFIA bigenic mice using an endothelial-specific antibody, VWF, which stains endothelial cells (Fig. 6*F-H*). Analysis of these sections revealed numerous blood vessels in all mammary glands examined, some of which were large (Fig. 6*F, arrowhead*) and some of which were small (Fig. 6*F, arrow*) and typically associated with epithelial structures. Although there was no significant difference in the number of large (>20 μm in diameter) blood vessels between the genotypes (Fig. 6*H*), there was a significant increase in the number of small blood vessels (<20 μm in diameter) in mammary glands from iFGFR1 transgenic mice. These smaller blood vessels seemed

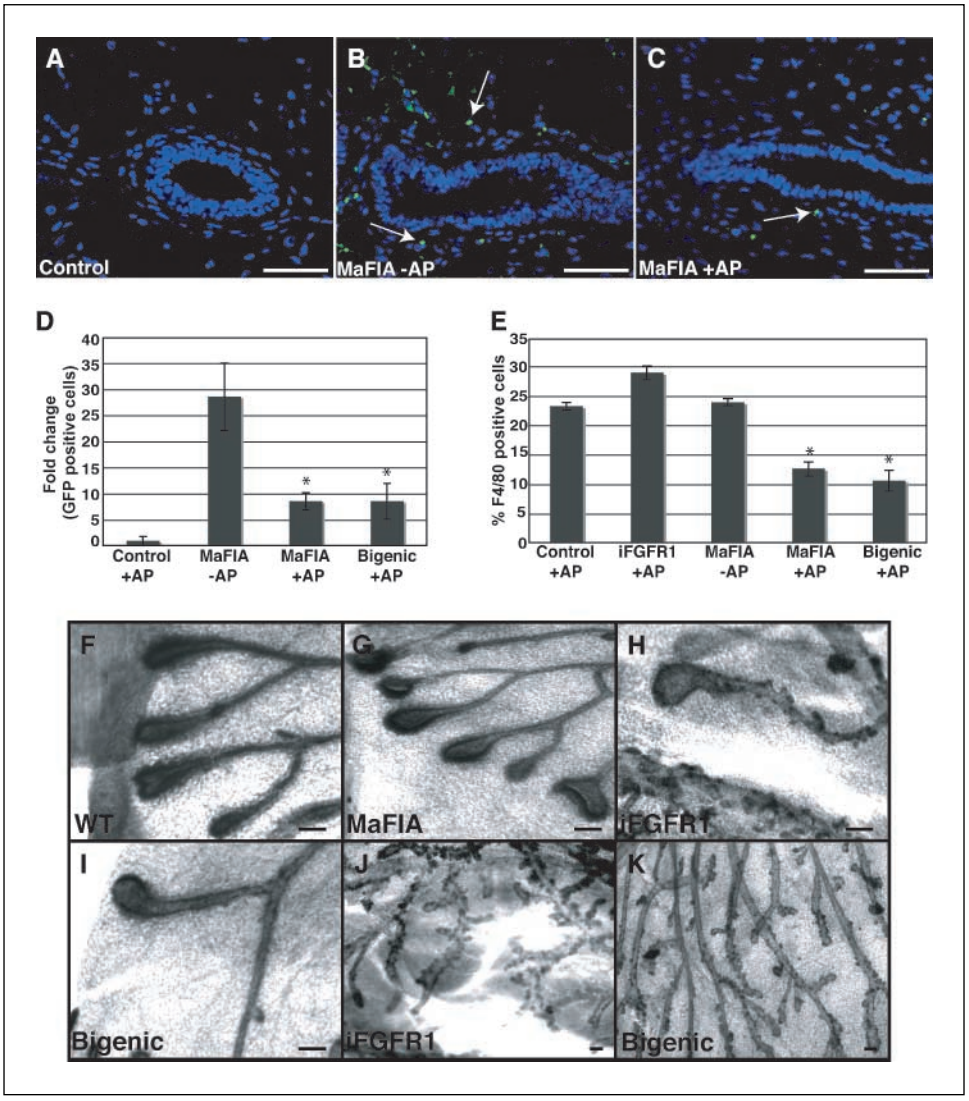

Figure 5. Decreased lateral bud progression in iFGFR1/MaFIA bigenic mice treated with AP20187. *A,* GFP staining of mammary gland section from nontransgenic mice (*Control*). *B,* GFP staining of a mammary gland section from a nontreated (*−AP*) MaFIA transgenic mouse. *Arrows,* GFP-expressing cells in the stroma surrounding the epithelium. *C,* GFP staining of a mammary gland section from MaFIA transgenic mouse treated with dimerizer (*+AP*). *Arrow,* presence of a GFP-positive cell in the stroma surrounding the epithelium. Bar, 50 μm. *D,* quantitation of the percentage depletion of GFP-expressing cells in mammary glands from MaFIA transgenic and iFGFR1/MaFIA bigenic mice without (*−AP*) and with (*+AP*) dimerizer treatment ($n = 3$ mice per genotype). *Bars,* SE. *, $P < 0.05$, significant decrease in GFP-positive cells in mammary glands from treated MaFIA and bigenic mice (paired *t* test). *E,* quantitation of F4/80-positive cells as determined by FACS analysis from nontransgenic, iFGFR1, MaFIA, and iFGFR1/MaFIA bigenic mice without (*−AP*) and with (*+AP*) dimerizer treatment ($n = 3$ mice per genotype). *Bars,* SE. *, $P < 0.05$, significant decrease in F4/80-positive cells in mammary glands from treated MaFIA and bigenic mice (paired *t* test). *F* to *K,* mammary gland whole mounts from dimerizer-treated WT mouse ($n = 4$; *F*), MaFIA transgenic mouse ($n = 4$; *G*), iFGFR1 transgenic mouse ($n = 6$; *H* and *J*), and iFGFR1/MaFIA transgenic mouse ($n = 6$; *I* and *K*) showing the effects of dimerizer treatment on TEBs (*F-I*) and subtending ducts (*J* and *K*). Bar, 200 μm.

DOI:10.1158/0008-5472.CAN-05-3781

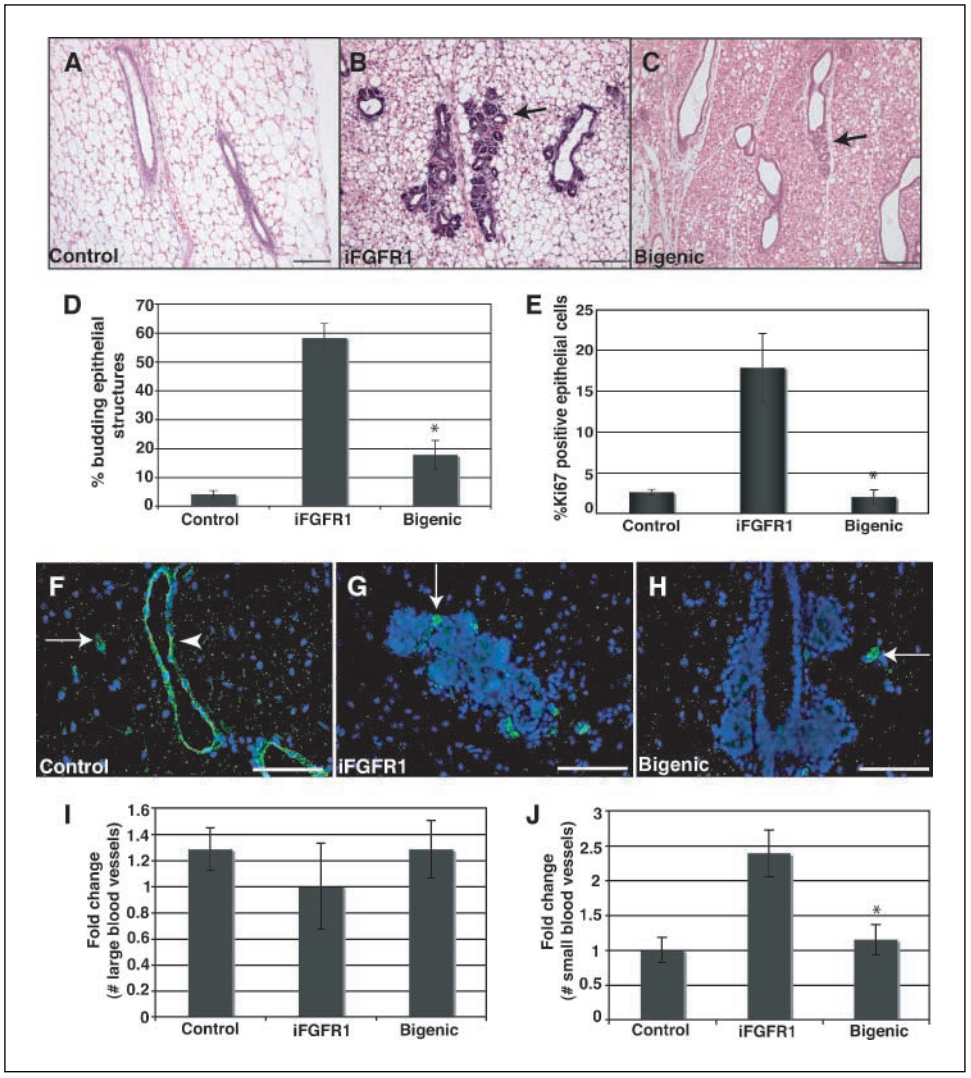

Figure 6. Macrophage depletion results in decreased iFGFR1-induced epithelial budding and angiogenesis. *A* to *C,* histologic analysis of mammary glands from nontransgenic (*A*), iFGFR1 transgenic (*B*), and iFGFR1/MaFIA bigenic (*C*) mice ($n = 3$ mice per genotype). *Arrows,* lateral epithelial budding. Bar, 100 μm. *D,* quantitation of epithelial structures that exhibit a budding phenotype expressed as a percentage of the total number of epithelial structures. *Bars,* SE. *, $P < 0.0001$, significant decrease in the percentage of epithelial budding structures in mammary glands from treated iFGFR1/MaFIA mice (paired *t* test). *E,* quantitation of Ki67-positive epithelial cells in mammary gland sections from control, iFGFR1, and iFGFR1/MaFIA mice following 9 days of dimerizer treatment. *Bars,* SE. *, $P < 0.01$, significant decrease in the percentage of Ki67-positive epithelial cells in mammary glands from treated iFGFR1/MaFIA mice (paired *t* test). *F* to *G,* immunofluorescence for VWF in mammary glands from nontransgenic ($n = 3$; *F*), iFGFR1 transgenic ($n = 3$; *G*), and iFGFR1/MaFIA bigenic mice ($n = 6$). *Arrowhead,* large blood vessel; *arrows,* small blood vessels. Bar, 100 μm. *H,* quantitation of the number of large blood vessels (>20 μm) in mammary glands from nontransgenic, iFGFR1, and iFGFR1/MaFIA bigenic mice. *Bars,* SE. *I,* quantitation of the number of small blood vessels (<20 μm) in mammary glands from nontransgenic, iFGFR1, and iFGFR1/MaFIA bigenic mice. *Bars,* SE. *, $P < 0.01$, significant decrease in the numbers of small blood vessels in mammary glands from treated iFGFR1/MaFIA mice (paired *t* test).

to be associated primarily with epithelial structures and clusters of lateral budding structures (Fig. 6*G, arrow*). Although there were also small blood vessels observed in mammary glands from the iFGFR1/MaFIA transgenic mice in close proximity to the lateral buds (Fig. 6*H, arrow*), there was a significant decrease ($P < 0.01$) in the number of these blood vessels (Fig. 6*I*), suggesting that macrophages are involved in mediating iFGFR1-induced angiogenesis.

Discussion

The results presented in this study expand on previous studies of the MMTV-iFGFR1 transgenic mice, which showed the utility of this model in analyzing early progression from hyperproliferative to invasive lesions in the mammary gland (14). To further characterize the early events contributing this process, microarray analysis was done. These analyses revealed several genes involved in the defense response, including genes involved in the recruitment of macrophages, which prompted us to analyze macrophage recruitment in the mammary gland following iFGFR1 activation. Interestingly, there seemed to be a rapid increase in the association of macrophages with the ducts and budding epithelial structures. Furthermore, macrophages continued to associate with alveolar hyperplasias after longer term (4 weeks) of dimerizer treatment, and their localization seemed to be similar to that of macrophages associated with alveolar buds during pregnancy. This observation suggests that macrophages may be involved in common mechanisms that are involved in both pregnancy-induced alveolar budding and iFGFR1-mediated budding, such as angiogenesis, migration, and proliferation.

Although several other chemokines involved in recruiting inflammatory cells were induced, including chemokines for neutrophils (Ccr5) and lymphocytes (Cxcl10 and Cxcl13), further analysis did not reveal significant recruitment of other inflammatory cells to the epithelial structures. However, recent studies using K14-HPV16 mice, which are a model for epithelial carcinogenesis, have shown that although B cells are not recruited to the tumors, soluble mediators synthesized by peripheral B cells are required for formation of the carcinomas (23). Therefore, the lack of inflammatory cells surrounding the epithelial structures does not necessarily negate a role for these cells in this model. Analysis of soluble mediators, such as immunoglobulins (23), surrounding the lateral buds and hyperplasias might show a further role for the adaptive immune system in the iFGFR1-induced phenotype.

DOI:10.1158/0008-5472.CAN-05-3781

Recruitment of tumor-associated macrophages (TAM) to tumors can be mediated by various processes, including hypoxia and chemokines secreted by tumor cells (24). Due to the rapid recruitment of macrophages, before the development of tumors that contain hypoxic regions, it is likely that the macrophage recruitment in the iFGFR1 model is being induced by a secreted factor derived from the mammary epithelial cells. A role for secreted growth factors in establishing a paracrine loop between mammary tumor cells and macrophages has been described in both cell culture and mouse models (25, 26). These studies showed that the mammary tumor cells secrete colony-stimulating factor-1 (CSF-1), which attracts macrophages, and the macrophages secrete EGF, which then acts on the tumor cells. It is possible that a similar regulatory loop exists between iFGFR1-expressing epithelial cells and macrophages; however, quantitative RT-PCR analysis did not show an increase in CSF-1 expression following iFGFR1 activation (data not shown).

Induction of another known macrophage chemoattractant, osteopontin, was identified following 8 hours of dimerizer treatment. Osteopontin is a secreted glycophosphoprotein that binds CD44 and integrins and is involved in mediating many aspects of tumor progression and metastasis (27). Osteopontin has been identified previously as a downstream target of iFGFR1 signaling in prostate cancer cells (28) and has also been shown to be induced by FGFR1 in rat aortic smooth muscle cells (29). Analysis of iFGFR1-induced osteopontin in mammary epithelial cells showed that secreted osteopontin-induced macrophage migration in a cell culture-based migration assay, suggesting that this is a potential mechanism by which macrophages are being recruited by epithelial cells expressing activated iFGFR1 *in vivo*. However, it is possible that macrophage recruitment *in vivo* may be induced by a combination of factors in addition to osteopontin. Previous studies using MMTV-c-myc/MMTV-v-Ha-ras transgenic mice showed that osteopontin expression was not required for the development of spontaneous mammary tumors, although these tumors secreted high levels of osteopontin (30), suggesting that other CD44 and integrin-binding ligands may be compensating for the loss of osteopontin.

To determine how macrophages might be influencing the iFGFR1-induced mammary phenotype, the MaFIA conditional macrophage ablation model was used. Analysis of iFGFR1/MaFIA bigenic mice treated with dimerizer clearly shows that macrophage reduction in the mammary gland affected the ability of the lateral buds to progress and inhibited iFGFR1-induced epithelial cell proliferation and angiogenesis. Studies in other models have shown a role for TAMs in inducing angiogenesis. For example, macrophages are known to express matrix metalloproteinase (MMP)-9, which may act to induce the mobilization of vascular endothelial growth factor (VEGF), resulting in the induction of local angiogenesis (31, 32). Although it has been well documented that activation of FGF signaling itself can induce expression and activation of MMPs and angiogenic factors (6, 33–35), the results of these studies suggest that macrophages are critical mediators of iFGFR1-induced angiogenesis in this system.

Studies of human breast cancer have shown that increased TAM density predicts poor prognosis and is associated with increased VEGF expression and microvessel density (36, 37), suggesting that macrophages may be involved in tumor angiogenesis. However, the role of macrophages in promoting neovascularization or other processes involved in early stage breast tumors, such as atypical ductal hyperplasia or ductal carcinoma *in situ*, has not been well established. Studies focusing on the recruitment of macrophages to early stages of breast tumors as well as the types of macrophages associated with these lesions may establish the importance of inflammatory cells in breast cancer progression and provide critical information for developing therapeutic strategies to target these cells.

Acknowledgments

Received 10/19/2005; revised 2/24/2006; accepted 4/4/2006.

Grant support: NIH grant CA16303, Ruth L. Kirschstein National Research Service Award grant CA 097676 (K.L. Schwertfeger), and Department of Defense Breast Cancer Research Fellowship grant DAMD 17-02-1-0285 (W. Xian).

The costs of publication of this article were defrayed in part by the payment of page charges. This article must therefore be hereby marked *advertisement* in accordance with 18 U.S.C. Section 1734 solely to indicate this fact.

We thank Shirley Small and Maria Gonzalez-Rimbau for technical support, Dr. David Spencer for comments on the article, and Dr. Dan Medina for help with histologic analysis. The MPIIIB10$_1$ monoclonal antibody developed by M. Solursh and A. Franzen was obtained from the Developmental Studies Hybridoma Bank developed under the auspices of the National Institute of Child Health and Human Resources (Bethesda, MD) and maintained by the Department of Biological Sciences, University of Iowa.

References

1. Ronnov-Jessen L, Petersen OW, Bissell MJ. Cellular changes involved in conversion of normal to malignant breast: importance of the stromal reaction. Physiol Rev 1996;76:69–125.
2. Bhowmick NA, Neilson EG, Moses HL. Stromal fibroblasts in cancer initiation and progression. Nature 2004;432:332–7.
3. Balkwill F, Charles KA, Mantovani A. Smoldering and polarized inflammation in the initiation and promotion of malignant disease. Cancer Cell 2005;7:211–7.
4. Pollard JW. Tumour-educated macrophages promote tumour progression and metastasis. Nat Rev Cancer 2004;4:71–8.
5. Ornitz DM. FGFs, heparan sulfate, and FGFRs: complex interactions essential for development. BioEssays 2000;22:108–12.
6. Presta M, Dell'era P, Mitola S, Moroni E, Ronca R, Rusnati M. Fibroblast growth factor/fibroblast growth factor receptor system in angiogenesis. Cytokine Growth Factor Rev 2005;16:159–78.
7. Grose R, Dickson C. Fibroblast growth factor signaling in tumorigenesis. Cytokine Growth Factor Rev 2005;16:179–86.
8. Callahan R, Smith GH. MMTV-induced mammary tumorigenesis: gene discovery, progression to malignancy, and cellular pathways. Oncogene 2000;19:992–1001.
9. Peters G, Brookes S, Smith R, Dickson C. Tumorigenesis by mouse mammary tumor virus: evidence for a common region for provirus integration in mammary tumors. Cell 1983;33:369–77.
10. Peters G, Brookes S, Smith R, Placzek M, Dickson C. The mouse homolog of the hst/k-FGF gene is adjacent to int-2 and is activated by proviral insertion in some virally induced mammary tumors. Proc Natl Acad Sci U S A 1989;86:5678–82.
11. MacArthur CA, Shankar DB, Shackleford GM. Fgf-8, activated by proviral insertion, cooperates with the Wnt-1 transgene in murine mammary tumorigenesis. J Virol 1995;69:2501–7.
12. Marsh SK, Bansal GS, Zammit C, et al. Increased expression of fibroblast growth factor 8 in human breast cancer. Oncogene 1999;18:1053–60.
13. Koziczak M, Holbro T, Hynes NE. Blocking of FGFR signaling inhibits breast cancer cell proliferation through downregulation of D-type cyclins. Oncogene 2004;23:3501–8.
14. Welm BE, Freeman KW, Chen M, Contreras A, Spencer DM, Rosen JM. Inducible dimerization of FGFR1: development of a mouse model to analyze progressive transformation of the mammary gland. J Cell Biol 2002;157:703–14.
15. Burnett SH, Kershen EJ, Zhang J, et al. Conditional macrophage ablation in transgenic mice expressing a Fas-based suicide gene. J Leukoc Biol 2004;75:612–23.
16. Seagroves TN, Krnacik S, Raught B, et al. C/EBPβ, but not C/EBPα, is essential for ductal morphogenesis, lobuloalveolar proliferation, and functional differentiation in the mouse mammary gland. Genes Dev 1998;12:1917–28.
17. Grimm SL, Contreras A, Barcellos-Hoff MH, Rosen JM. Cell cycle defects contribute to a block in hormone-induced mammary gland proliferation in CCAAT/enhancer-binding protein (C/EBPβ)-null mice. J Biol Chem 2005;280:36301–9.
18. Yuen T, Zhang W, Ebersole BJ, Sealfon SC. Monitoring G-protein-coupled receptor signaling with DNA microarrays and real-time polymerase chain reaction. Methods Enzymol 2002;345:556–69.
19. Livak KJ, Schmittgen TD. Analysis of relative gene expression data using real-time quantitative PCR and the 2(−ΔΔC(T)) method. Methods 2001;25:402–8.

DOI:10.1158/0008-5472.CAN-05-3781

20. Gouon-Evans V, Rothenberg ME, Pollard JW. Postnatal mammary gland development requires macrophages and eosinophils. Development 2000;127:2269–82.

21. Ball RK, Friis RR, Schoenenberger CA, Doppler W, Groner B. Prolactin regulation of β-casein gene expression and of a cytosolic 120-kd protein in a cloned mouse mammary epithelial cell line. EMBO J 1988;7:2089–95.

22. Nunohiro T, Ashizawa N, Graf K, Hsueh WA, Yano K. Angiotensin II promotes integrin-mediated collagen gel contraction by adult rat cardiac fibroblasts. Jpn Heart J 1999;40:461–9.

23. de Visser KE, Korets LV, Coussens LM. *De novo* carcinogenesis promoted by chronic inflammation is B lymphocyte dependent. Cancer Cell 2005;7:411–23.

24. Bingle L, Brown NJ, Lewis CE. The role of tumour-associated macrophages in tumour progression: implications for new anticancer therapies. J Pathol 2002;196:254–65.

25. Wyckoff J, Wang W, Lin EY, et al. A paracrine loop between tumor cells and macrophages is required for tumor cell migration in mammary tumors. Cancer Res 2004;64:7022–9.

26. Goswami S, Sahai E, Wyckoff JB, et al. Macrophages promote the invasion of breast carcinoma cells via a colony-stimulating factor-1/epidermal growth factor paracrine loop. Cancer Res 2005;65:5278–83.

27. Wai PY, Kuo PC. The role of osteopontin in tumor metastasis. J Surg Res 2004;121:228–41.

28. Freeman KW, Gangula RD, Welm BE, et al. Conditional activation of fibroblast growth factor receptor (FGFR) 1, but not FGFR2, in prostate cancer cells leads to increased osteopontin induction, extracellular signal-regulated kinase activation, and *in vivo* proliferation. Cancer Res 2003;63:6237–43.

29. Li G, Oparil S, Kelpke SS, Chen YF, Thompson JA. Fibroblast growth factor receptor-1 signaling induces osteopontin expression and vascular smooth muscle cell-dependent adventitial fibroblast migration *in vitro*. Circulation 2002;106:854–9.

30. Feng F, Rittling SR. Mammary tumor development in MMTV-c-myc/MMTV-v-Ha-ras transgenic mice is unaffected by osteopontin deficiency. Breast Cancer Res Treat 2000;63:71–9.

31. Bergers G, Brekken R, McMahon G, et al. Matrix metalloproteinase-9 triggers the angiogenic switch during carcinogenesis. Nat Cell Biol 2000;2:737–44.

32. Giraudo E, Inoue M, Hanahan D. An amino-bisphosphonate targets MMP-9-expressing macrophages and angiogenesis to impair cervical carcinogenesis. J Clin Invest 2004;114:623–33.

33. Pintucci G, Yu PJ, Sharony R, et al. Induction of stromelysin-1 (MMP-3) by fibroblast growth factor-2 (FGF-2) in FGF-$2^{-/-}$ microvascular endothelial cells requires prolonged activation of extracellular signal-regulated kinases-1 and -2 (ERK-1/2). J Cell Biochem 2003;90:1015–25.

34. Suyama K, Shapiro I, Guttman M, Hazan RB. A signaling pathway leading to metastasis is controlled by N-cadherin and the FGF receptor. Cancer Cell 2002;2:301–14.

35. Xian W, Schwertfeger KL, Vargo-Gogola T, Rosen JM. Pleiotropic effects of FGFR1 on cell proliferation, survival, and migration in a 3D mammary epithelial cell model. J Cell Biol 2005;171:663–73.

36. Tsutsui S, Yasuda K, Suzuki K, Tahara K, Higashi H, Era S. Macrophage infiltration and its prognostic implications in breast cancer: the relationship with VEGF expression and microvessel density. Oncol Rep 2005;14:425–31.

37. Yu JL, Rak JW. Host microenvironment in breast cancer development: inflammatory and immune cells in tumour angiogenesis and arteriogenesis. Breast Cancer Res 2003;5:83–8.